Electrochimica Acta 56 (2011) 6866–6873

Contents lists available at ScienceDirect

Electrochimica Acta

journal homepage: www.elsevier.com/locate/electacta

Pulsed electrodeposition of p-type $CuInSe_2$ thin films

M.H. Valdés, M. Vázquez *,[1]

División Corrosión, INTEMA, Facultad de Ingeniería, CONICET-Universidad Nacional de Mar del Plata - Juan B. Justo 4302 – B7608FDQ Mar del Plata, Argentina

ARTICLE INFO

Article history:
Received 30 March 2011
Received in revised form 23 May 2011
Accepted 27 May 2011
Available online 6 June 2011

Keywords:
Pulsed electrodeposition
$CuInSe_2$
Annealing
Etching

ABSTRACT

$CuInSe_2$ thin films have been electrodeposited on conductive glass using cyclic pulse electrodeposition. One cycle consists of consequtively applying potentials E_1 and E_2, each during 10 s and a total of 90 cycles are applied. E_1 is chosen between −0.7 and −0.9 V_{SCE} while E_2 is fixed at −0.1 V_{SCE}. The films are annealed in argon and then etched in KCN solution to eliminate remnant secondary phases. The material is characterized employing grazing incident X-rays diffraction, Raman spectroscopy, scanning electron microscopy and energy dispersive scanning spectroscopy. The presence of secondary phases seems to be reduced when compared to films prepared at fixed potentials. The films are crystalline and the overall quality improves by annealing in Ar. Photoelectrochemical tests, Mott–Schottky plots and *I–V* curves confirm p-type conduction. The diffusion regime imposed by the potential pulses could be responsible for the different morphology and composition of samples prepared with pulsed and potentiostatic electrodeposition.

1. Introduction

Copper indium selenides are very attractive materials for photovoltaic applications due to their high absorption coefficient, coupled to a band gap energy value matching the solar radiation.

Among the many techniques used to prepare $CuInSe_2$ (CISe) as a thin film, electrodeposition presents advantages: it is cost-effective, it does not require high vacuum, it can copy intricate geometries and can be done even on top of flexible substrates [1]. In particular, cyclic pulse electrodeposition is an attractive method to infiltrate nanoporous structures or templates [2,3], which constitutes a promising scenario when aiming at 3D solar cell configurations. Highly efficient, 3-D solar cells have been recently prepared infiltrating nanostructured TiO_2 with copper indium sulphides prepared using reactive pulses, like ALD or CVD [4,5]. There, the basic components are delivered to the substrate in gaseous reactive cycles. One important disadvantage of these techniques is the high production costs, which complicate large scale production of solar cells.

However, some problems associated to electrodeposition have yet to be overcome. The instability of the electrodeposition bath over long periods of time can be tackled using complexing agents [6,7]. Also, the generation of secondary phases, such as Cu_xSe, is a well-known disadvantage, which is usually solved by etching with KCN [1,8]. Finally, the crystallinity of the films needs to be improved by annealing. But due to the low vapor pressure of Se, films annealed in vacuum, nitrogen or argon atmospheres usually present high levels of Se vacancies. For this reason, selenization may be necessary to replace the lost selenium and to adjust the final stoichiometry of the CISe films [9,10]. However, the high toxicity of gaseous Se can be a limitation for mass production of CISe-devices. So, even when all these are efficient solutions, they impose serious environmental issues and increase costs.

This investigation addresses the benefits of pulsed-electrodeposition, as it may contribute in adjusting the composition of the films [11–13], while producing crystalline layers. Thus, the crystallographic, compositional, optical and morphological properties of $CuInSe_2$ are studied. In the near future, the viability of infiltrating nanoestructures of TiO_2 with CISe electrodeposited by pulsing the potential will be explored.

2. Experimental

$CuInSe_2$ (CISe) was deposited by cyclic pulse electrodeposition from a single bath. Glass coated with fluorine-doped tin oxide is used as substrate (Pilkington TEC Glass™, TEC 8, $\rho \sim 8\ \Omega$/sq). The substrate was cleaned and rinsed as described earlier [14]. The geometrical area was 1.13 cm^2.

A three-electrode cell, with a Pt mesh as counter electrode and a saturated calomel electrode (SCE) as reference electrode, was used. The electrodepositions were performed employing a PGP 201 Voltalab® potentiostat/galvanostat.

The precursor electrolyte was an aqueous solution containing 2.5 mmol L^{-1} $CuCl_2$, 10 mmol L^{-1} $InCl_3$ and 5 mmol L^{-1} SeO_2 with 0.2 mol L^{-1} KCl as supporting electrolyte. The pH was adjusted

* Corresponding author. Tel.: +54 223 481 6600x244; fax: +54 223 481 0046.
E-mail address: mvazquez@fi.mdp.edu.ar (M. Vázquez).
[1] 1. ISE active member.

0013-4686/$ – see front matter © 2011 Elsevier Ltd. All rights reserved.
doi:10.1016/j.electacta.2011.05.108

Table 1
Average thicknesses calculated using Faraday's law.

Electrodeposition	Potential (V vs SCE)	Thickness (μm)
Pulsed	−0.7	0.398
Pulsed	−0.9	0.662
Potentiostatic	−0.7	0.711
Potentiostatic	−0.9	1.017

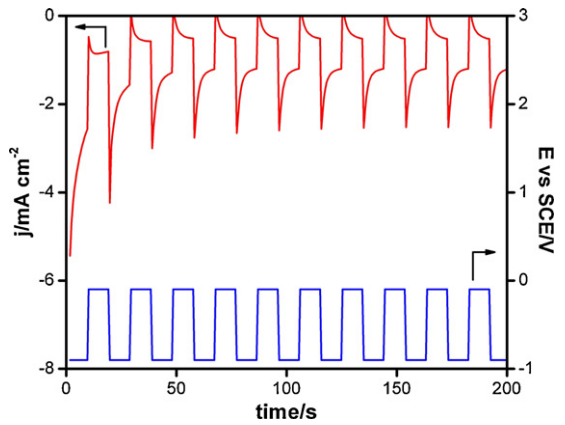

Fig. 1. Potential–pulse profile imposed during the deposition of CISe films and the corresponding current–time response.

between 2.0 and 2.5 with a few drops of a concentrated HCl stock solution.

When using potentiostatic electrodeposition, two potential values were used: −0.7 and −0.9 V_{SCE}. The deposition time is always 30 min and the solution is purged with nitrogen to remove the oxygen from the electrolyte before the electrodeposition. After completing the electrodeposition, the samples are rinsed with distilled water and dried in air. The average thicknesses attained were evaluated using Faraday's law and are presented in Table 1.

When using cyclic pulsed electrodeposition, one pulse consisted of applying E_1 for 10 s and then E_2 for another 10 s. Two E_1 values were investigated, −0.7 and −0.9 V_{SCE} and E_2 was fixed at −0.1 V_{SCE}, initially following the potentials previously reported in the literature [11]. A typical response (i vs. t) is presented in Fig. 1. 90 cycles were applied, which took 1800s. Average thicknesses are shown in Table 1.

The films were annealed in argon at 500 °C during 30 min, using a home-built reactor. When indicated, CISe films were chemically etched by immersing the sample in 0.5 mol L^{-1} KCN during 5 min.

The crystalline structure of the films was analyzed by X-ray diffraction in grazing incidence configuration (GXRD) using a PANalytical X'Pert PRO diffraction system employing Cu-Kα radiation at 40 kV and 40 mA. The samples were scanned between 15° and 75° with a step size of 0.01°, with a 3° incidence angle. The crystallographic data for each phase were taken from the literature [15].

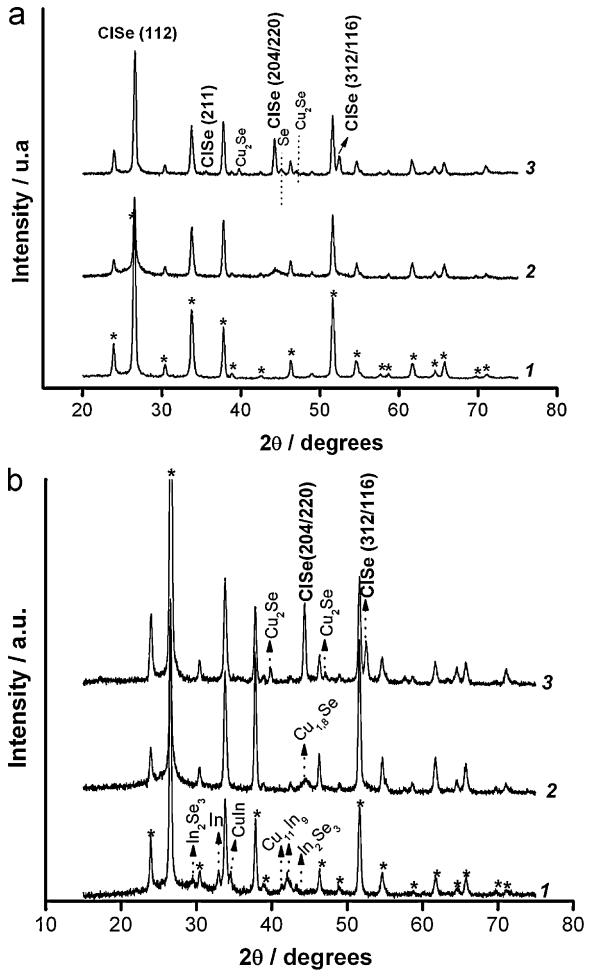

Fig. 2. GXRD diffractogram of electrodeposited CISe films.
(a) Pulsed electrodeposition, 90 cycles at $E_1 = -0.7\ V_{SCE}$. (1) FTO substrate; (2) as deposited; (3) annealed in argon at 500 °C for 30 min.
(b) Electrodeposition, at $E/E_1 = -0.9\ V_{SCE}$. (1) Pulsed electrodeposition, 90 cycles, as deposited samples; (2) potentiostatic electrodeposition, 1800s, as deposited samples; (3) pulsed electrodeposition, 90 cycles, annealed samples.

Raman spectroscopy measurements were performed using an Invia Reflex confocal Raman microprobe using a 50× objective. Excitation was provided with the 514 nm emission line of an Ar^+ laser. To prevent damage by heating, the power of the laser was reduced to 10% using neutral density filters. In this configuration the laser power on the sample was 0.2 mW measured with a silicon photodiode (Coherent Inc.). For these power conditions, no observable thermal effects on the Raman spectra were found.

Table 2
Chemical composition of different as-deposited electrodeposited CISe films, determined by EDS.

	Cycles	Cu	In	Se	Cu/In	Se/(Cu + In)
As deposited						
−0,7 V_{SCE}	Yes	21,32	17,41	61,27	1,22	1,58
−0,9 V_{SCE}	Yes	20,74	21,04	58,22	0,99	1,39
−0,7 V_{SCE}	No	23,53	23,48	52,99	1	1,13
−0,9 V_{SCE}	No	21,39	48,95	29,66	0,44	0,42
Annealed Ar (500 °C–30 min)						
−0,7 V_{SCE}	Yes	22,33	16,25	61,42	1,37	1,59
−0,9 V_{SCE}	Yes	22,58	21,88	55,54	1,03	1,25
Annealed + KCN etching						
−0,9 V_{SCE}	Yes	23,31	21,78	54,90	1,07	1,22

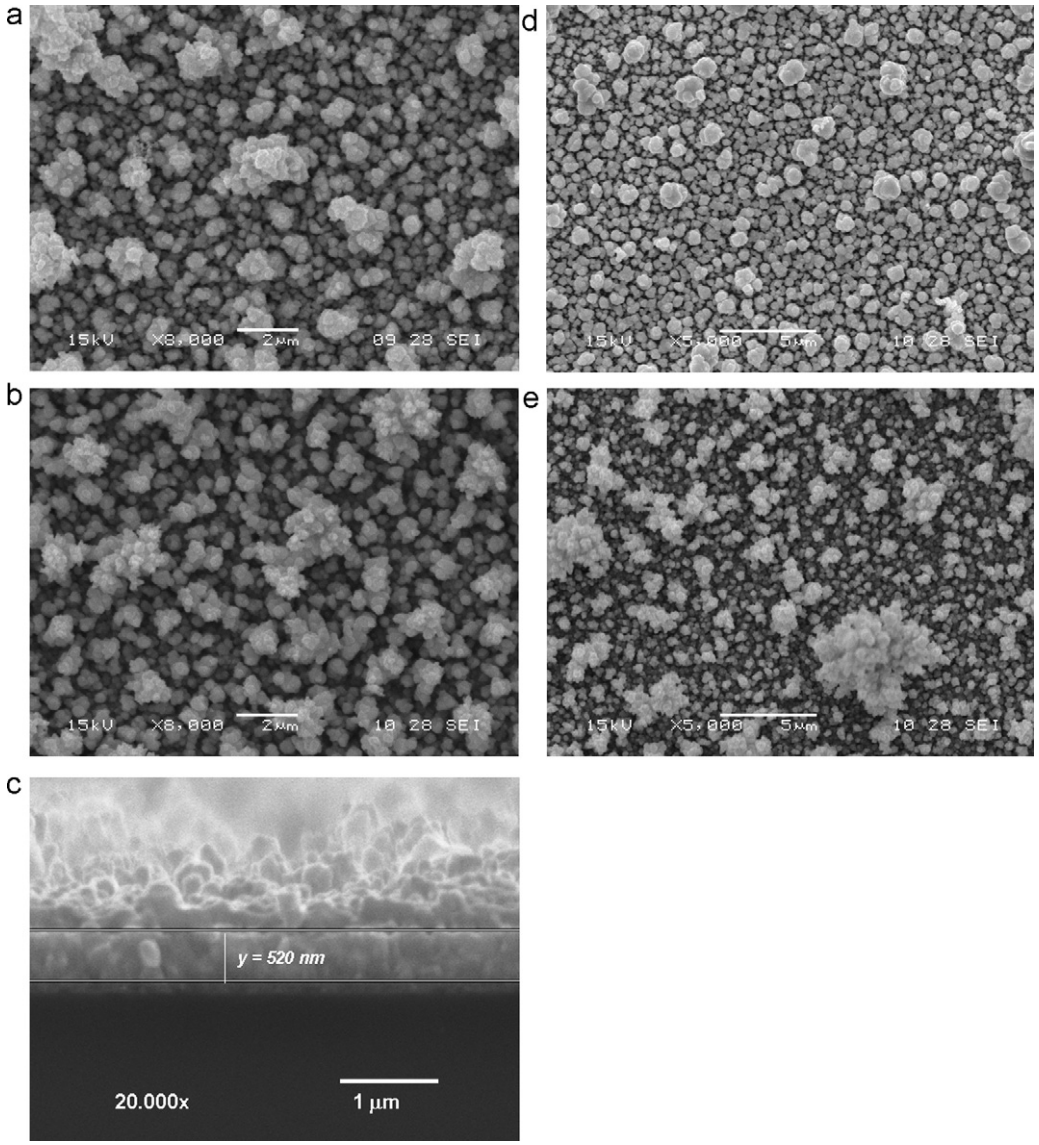

Fig. 3. SEM images of CISe electrodeposited films, prepared by pulsing the potential.
(1) As-deposited samples (a) $E_1 = -0.7\ V_{SCE}$; (b) $E_1 = -0.9\ V_{SCE}$; (c) $E_1 = -0.9\ V_{SCE}$, cross view; (2) Samples annealed for 30 min at 500 °C in Ar. (d) $E_1 = -0.7\ V_{SCE}$; (e) $E_1 = -0.9\ V_{SCE}$.

Film morphology and composition was studied by SEM and EDS, with a scanning electron microscope JEOL JSM-6460LV coupled with an EDAX Genesis XM4 – Sys 60 Multichannel Analyzer for X-ray Energy Dispersive Spectroscopy (EDS).

To calculate the thickness of the films (T), an equation based on Faraday's law has been used (Eq. (1)):

$$T = \frac{1}{nFA}\left(\frac{itM}{\rho}\right) \quad (1)$$

Here n is the number of electrons transferred, F is Faraday's number, A is the electrode geometrical area, i is the current, t is the deposition time, M is the formula weight, and ρ is the density. In the case of CISe, $M = 336.28$ g/mol and $\rho = 5.77$ g/cm^3. Also, 13 electrons are exchanged, as described by reaction (2):

$$Cu^{+2} + In^{+3} + 2SeO_3{}^{-2} + 12H^+ + 13e^- \rightarrow CuInSe_2 + 6H_2O \quad (2)$$

A Shimadzu UV-160A spectrophotometer was employed to register absorption spectra in the wavelength range 350–1100 nm at room temperature.

Photocurrent, photopotential and potentiodynamic measurements were carried out forming a semiconductor/electrolyte junction by immersion of the FTO/CISe film in 0.5 mol L^{-1} KCl solutions. The light source was a 150 W Xe lamp, chopped using an electronic shutter (Uniblitz^R model T132). The light beam entered the cell through a quartz window and shinned on the film side of the glass. A filter removes the ultraviolet radiation (Schott^{TM}, $\lambda < 350$ nm). An IVIUM$^®$ compact potentiostat/galvanostat was employed to carry out these measurements.

In the same experimental configuration Mott–Schottky analysis was undertaken by applying a 0.01 V_{rms} sinusoidal excitation signal with a frequency of 1 kHz. The applied bias ranges from 0.0 to −0.8 V, at a sweeping rate of 0.01 V s^{-1}, scanning the potential in the negative direction.

3. Results and discussion

Fig. 2 presents GXRD diffractograms of samples electrodeposited (ED) using pulsed and fixed potentials. Fig. 2a compares as-deposited and annealed CISe films prepared at $-0.7\ V_{SCE}$. A diffractogram of the FTO substrate is also superimposed for the sake of comparison. As can be seen, the substrate spectrum presents many peaks, most of them resulting from SnO_2 (identified with an

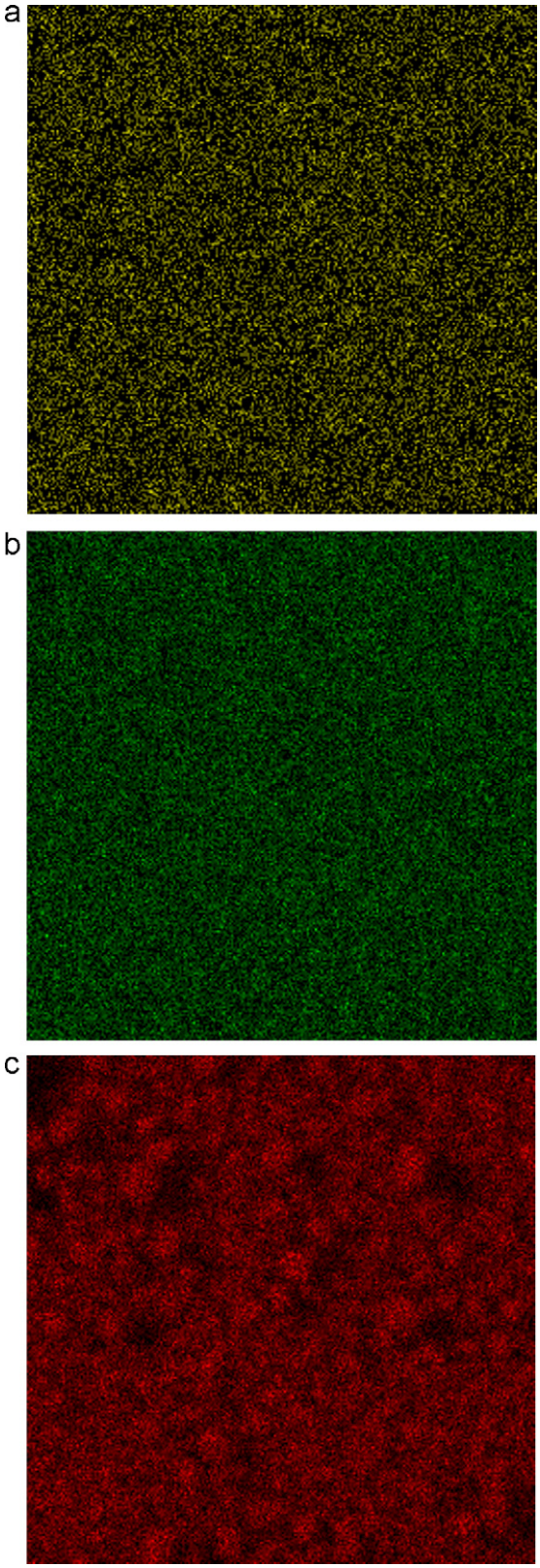

Fig. 4. EDS element mapping of CISe films. As-deposited samples, prepared by pulsing the potential. $E_1 = -0.9\,V_{SCE}$. (a), Cu map; (b) In map and (c) Se map.

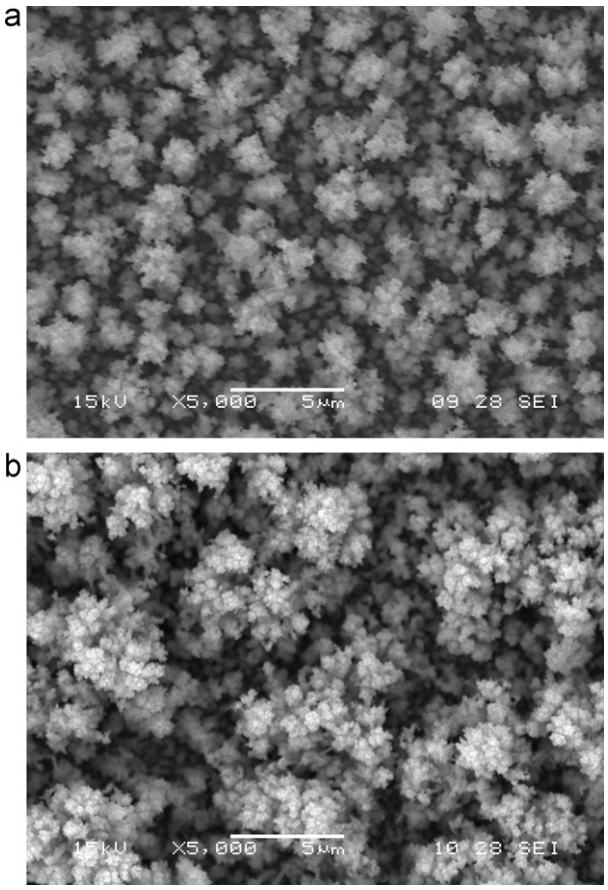

Fig. 5. SEM images of CISe electrodeposited films, prepared at constant potential. As-deposited samples. (a) $E = -0.7\,V_{SCE}$; (b) $E = -0.9\,V_{SCE}$.

asterisk, *). Unfortunately, the main (1 1 2) diffraction plane of CISe appears at the same angle than one of the components of FTO. However, it is clear that only after annealing other diffraction planes from the CISe phase like (2 0 4/2 2 0), (2 0 0/1 1 6) and (2 1 1) can be seen in the diffractogram, confirming the improvement of the film crystallinity. Also, it is worth noting that small reflections of undesirable phases such as Cu_2Se, and Se are now present. Fig. 2b shows diffractograms of samples prepared at $-0.9\,V_{SCE,}$ comparing potentiostatic and pulsed electrodeposition (with and without annealing). Again, the contribution of the main peak of CISe cannot be distinguished from that of FTO. However, the as-deposited

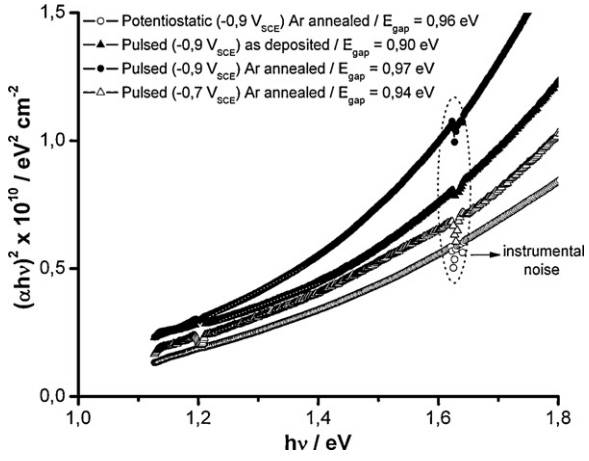

Fig. 6. Plots of $(\alpha h\nu)^2$ vs. $(h\nu)$, for CISe films comparing pulsed and potentiostatic deposition at -0.7 and $-0.9\,V_{SCE}$, with and without annealing.

sample prepared by pulsed electrodeposition shows a broad peak at 44.4° that could comprise the contribution of $Cu_{1.8}Se$ (main diffraction at 44.48°) and $CuInSe_2$ (diffraction at 44.27°). In parallel, the sample electrodeposited at fixed potential does not have this signal and shows peaks that can be attributed to In_2Se_3, $CuIn/Cu_9In_{11}$ alloys and metallic In, which are absent in the pulsed sample. The excess of indium in the global composition of this sample was confirmed by EDS (see below). Finally, as was the case for Fig. 2a, other diffraction planes from the CISe phase can be clearly identified after annealing the films.

Table 2 presents the composition of as-deposited, annealed and etched samples, as determined by EDS. When using pulsed electrodeposition, as-deposited samples are highly rich in selenium, in agreement with the XRD results. Others authors have found that an excess in selenium promotes the formation of Cu_xSe compunds [16,17]. However, as selenium is readily vaporized when the temperature increases, the annealing stage seems to improve the stoichiometry of the CISe layer, particularly in the film deposited at $-0.9\,V_{SCE}$. In this case, etching seems to produce no further improvement in the average composition of the film. When using potentiostatic electrodeposition, the as-deposited sample prepared at $-0.9\,V_{SCE}$ is highly rich in indium. This could be associated to the composition of the electrolytic bath, to the excessively negative potential, or both. XDR diffractograms confirm this result. In the case of the sample electrodeposited at $-0.7\,V_{SCE}$, the global composition seems to be well-adjusted to that of CISe. Nevertheless, it should be kept in mind that this analysis does not identify the different phases and for this reason, EDS has been complemented with X-ray diffractograms and Raman spectra.

Fig. 3 displays SEM micrographs of as-deposited samples, prepared by pulsing the potential with $E_1 = -0.7$ and $-0.9\,V_{SCE}$. There is no noticeable effect of the most negative potential of the pulse on the morphology of the resulting film. All the images show spherical, submicron-size grains, homogenously distributed and with a good coverage of the whole surface. SEM cross-sections resulted in good agreement with the thickness values given in Table 1. However, it is worth noticing that Eq. (1) should be taken as an approximation, since the formula weight and density vary with the composition, the area is not corrected by the surface roughness and the efficiency of electrodeposition rarely reaches 100%. Upon annealing, the films seem to be more compact, particularly in the case of the sample prepared with $E_1 = -0.7\,V_{SCE}$.

Cu, In and Se EDS mapping are shown in Fig. 4 and illustrate an even distribution of all the elements along the sample (only the results for the annealed film deposited at $E_1 = -0.7\,V_{SCE}$ are shown).

Fig. 5 presents SEM micrographs of as-deposited samples electrodeposited at fixed potentials (−0.7 and −0.9 V). Comparing Figs. 3 and 5, a remarkable change in morphology can be seen as a result of pulsing or fixing the potential. The films grown potentiostatically are porous and they present a cauliflower–like structure frequently found in electrodeposited CISe films [16,17]. Meanwhile, the films prepared by pulsed electrodeposition exhibit a more compact and homogenous coverage, which improves after annealing.

The band gap values (E_g) of semiconductor films were determined from transmittance spectra by plotting and extrapolating $(-\ln(T)\cdot h\nu)^2$ versus $(h\nu)$ after the annealing treatment, and are shown in Fig. 6. Results from potentiostatic and pulsed electrodeposition are compared. Independently of the preparation mode, the calculated E_g presents average values between 0.92 and 1.0 eV, in close agreement with values reported for CISe films obtained by three-potential pulsed electrodeposition [13] and by fixed potential deposition in different conditions [14,18]. The sample prepared pulsing the potential presents a band gap energy value closer to 1 eV. It is worth pointing out that no significant difference in the band gap energy value could be attributed to the use of various potentials or to the annealing stage.

In order to check the compositional homogeneity of the samples, Raman micro-mapping was performed by recording 29 spectra along the diagonal of $20 \times 20\,\mu m$ regions, which are presented in Fig. 7. Fig. 7a and b compare as-deposited CISe films prepared by pulsed ED ($E_1 = -0.9\,V_{SCE}$) and potentiostatic ED ($E = -0.9\,V_{SCE}$), respectively. In every spectrum, the most intense signal corresponds to the A_1 mode.

As discussed in the literature [19], the position of the peaks from the A_1 mode may be slightly blueshifted compared to the chalcopyrite $CuInSe_2$ A1 mode ($173\,cm^{-1}$), reflecting compressive residual stress.

Additional vibration modes typical of chalcopyrite are also present in the spectra [20]. At $128\,cm^{-1}$ the B_1 mode assigned to the vibration of Cu–In bonds and the low intensity band B_2, E between 200–230 cm^{-1} are present. Similar results were reported for CISe films prepared at fixed potentials deposited on dense TiO_2 layers [14]. It is clear from the comparison that the amount of binary Cu_xSe phases is greater in the sample prepared at fixed potential. In contrast, in the sample deposited using potential pulses, there is a signal at $240\,cm^{-1}$ that can be attributed to trigonal selenium [21]. This excess in Se could be related to the need of better adjusting the composition of the precursor solution when cycling the potential, which currently seems to favor the deposition of Se. Also, the composition of the sample prepared by pulsed ED is more homogenous. The film prepared using potentiostatic ED shows a greater contribution of the B_1 signal. This signal is absent in most of the spectra of films prepared by pulsed ED, and could be associated to the different morphology of the films and/or to the presence of In-rich phases.

Fig. 7c and d present micro-mapping of CISe films prepared by pulse ED. Both films were annealed in argon flux (500 °C – 30 min) but only one (Fig. 7d) was etched in KCN solution. First, it is worth noting that the composition of both films is clearly homogeneous. By comparing Fig. 7a and c it can be seen that the peaks are sharper after annealing, as expected for more crystalline samples. Also, it is worth noting that the signal attributed to the trigonal Se is no longer present in the annealed films. This confirms that Se is vaporized during the annealing stage, in agreement with the EDS results or incorporated to the structure of CISe. Both types of films present sharp signals of the A_1 mode indicating that the film is mainly composed by $CuInSe_2$. However, small lumps appear in the annealed samples in the region around $260\,cm^{-1}$ and these can be attributed to disperse Cu_xSe compounds that are still present in the film. In the case of the etched film, the region close to $260\,cm^{-1}$ is flatter which confirms the partial dissolution of the Cu_xSe secondary phase.

Fig. 7e and f show Raman spectra of annealed samples where the effect of the different preparation methods, potentials chosen and etching treatments can easily compared. The spectra have been normalized to the intensity of A_1 mode and displaced along the *Y*-axis for visual purposes. Clearly, the B_1 mode is absent in the samples prepared using pulsed potentials and etching effectively dissolves Cu_xSe compounds.

It is well known that the semiconducting properties of chalcopyrite depend on their non-stoichiometry and are governed by the presence of intrinsic defects such vacancies and interstitials [22,23]. It has been shown that the p-type films involve a slight excess of copper, whereas the n-type films involve excess of indium [24–26]. But even if the predominant type of conduction can depend on preparation methods, examples of n-type CISe prepared by pulsed electroplating have been reported before [25]. Photoelectrochemistry can be used to explore the nature of the carriers. When semiconductor electrodes are exposed to periodic illumination, the current driven is affected by the creation of electron–hole pairs, which alters the concentration of minority carriers and thereby promotes processes governed by these carriers. During photoex-

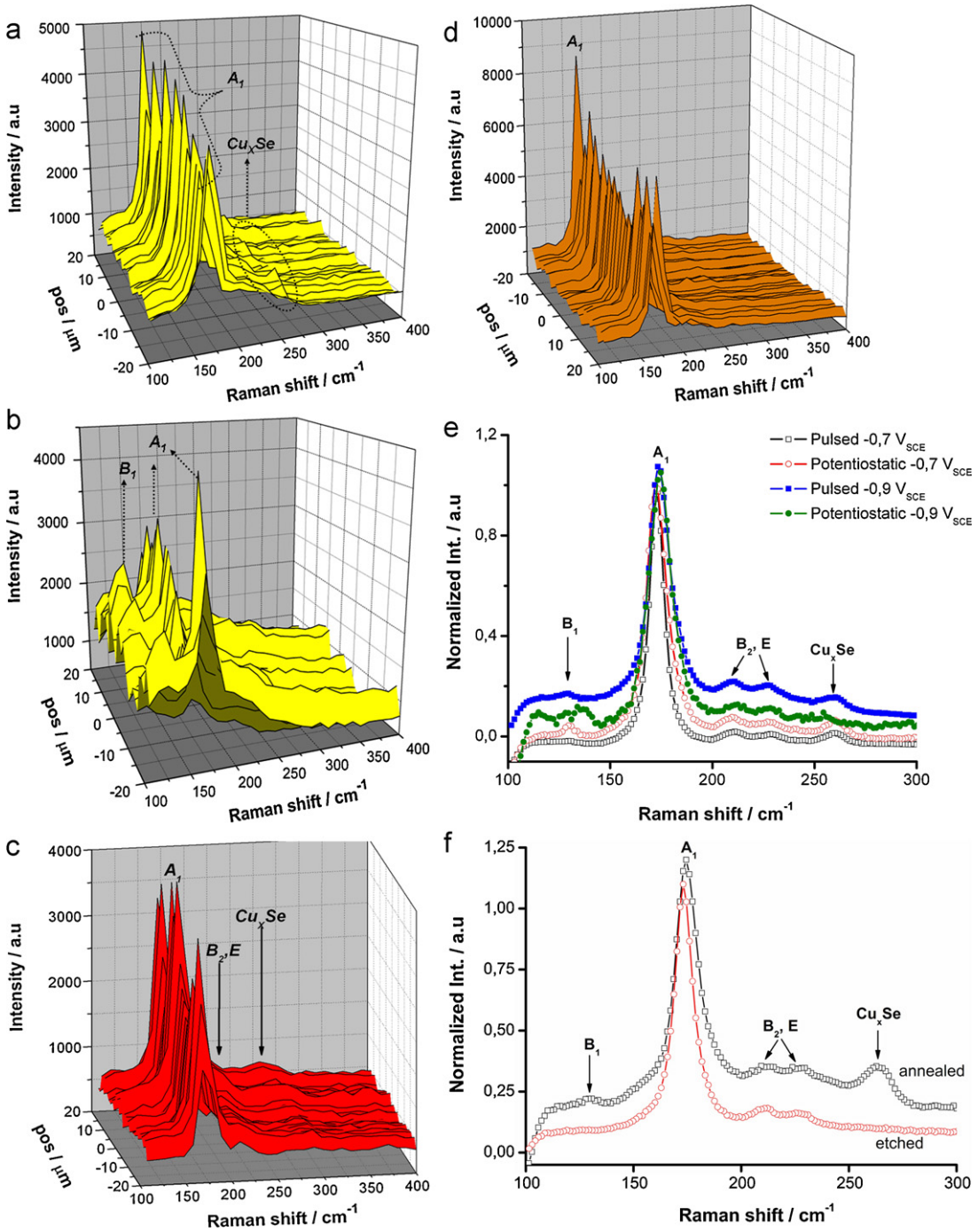

Fig. 7. Raman spectra of CISe prepared by electrodeposition, using $E/E_1 = -0.9\,V_{SCE}$. (a) and (b) micro-mapping of as-deposited CISe films comparing pulsed (a) and potentiostatic (b) electrodeposition; (c) and (d) micro-mapping of annealed CISe films (30 min at 500 °C) comparing samples with (c) and without (d) etching in KCN; (e) and (f) 2D Raman spectra of annealed CISe films (30 min at 500 °C) comparing (e) pulsed and potentiostatic deposition at −0.7 and $-0.9\,V_{SCE}$ and (f) with and without etching in KCN ($E_1 = -0.9\,V_{SCE}$).

citation, both photopotential and photocurrent can be observed, even at open circuit potential. The photoexcited electrons and holes are separated in the space charge layer, and are driven by the electric field in opposite directions. This migration induces an inverse potential in the electrode (photopotential), reducing the potential difference across the space charge layer and retarding the migration of the carriers. In the case of p-type semiconductors, the Fermi level of the semiconductor decreases (the electrode potential increases) when the band edge level bends downward in the space charge layer. Moreover, a negative photocurrent is registered when photoproduced electrons move across the space charge region towards the electrode/electrolyte interface and increase the cathodic current [27]. Fig. 8 shows the photocurrent registered at open circuit potential and the photopotential developed across the junction. The cathodic nature of the photocurrent and the positive value of the photopotential confirm the p-type character of the film. As it can be seen, the photocurrent of the films prepared at constant potential is lower.

To evaluate semiconductor parameters such as the flat band potential (V_{FB}) and the density of carriers, AC measurements can

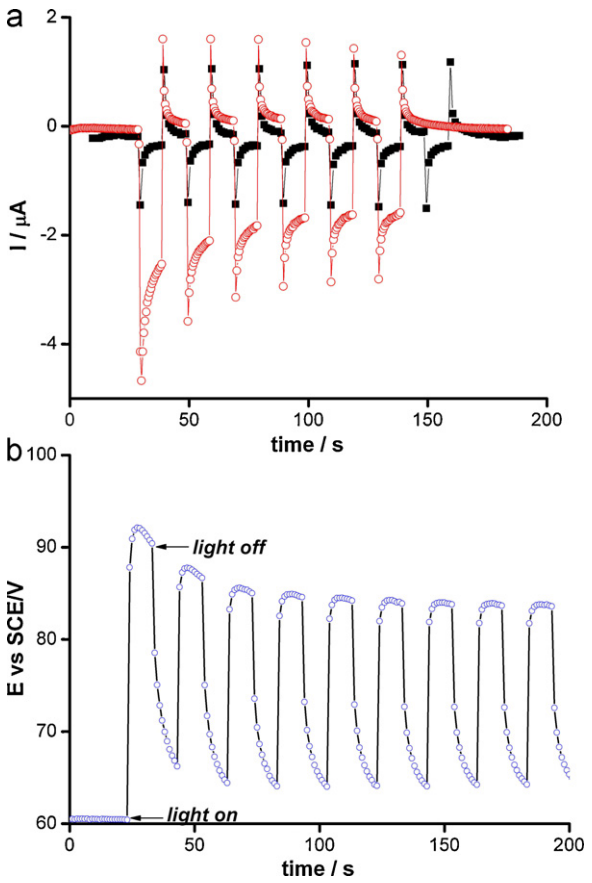

Fig. 8. Photocurrent (A) and photopotential (B) response of CISe films annealed in argon, using chopped light (10 s on/10 s off). Hollow symbols for CISe films prepared by pulsed electrodeposition, using $E_1 = -0.9\,V_{SCE}$. Solid symbols for CISe films prepared by potentiostatic electrodeposition, using $E = -0.9\,V_{SCE}$.

be interpreted from a Mott–Schottky (MS) plot (Eq. (3)):

$$\frac{1}{C^2} = \left(\frac{2}{e\varepsilon_0\varepsilon_r NA^2}\right)\left(V - V_{FB} - \frac{kT}{e}\right) \quad (3)$$

where C is the differential capacitance of the space-charge region, ε_0, the permittivity of vacuum, ε_r the relative dielectric constant, N the donor density for n-type semiconductor or the acceptor density

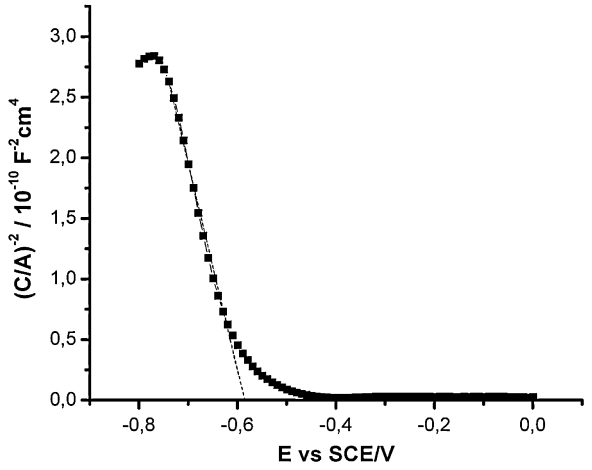

Fig. 9. Mott–Schottky plot of $CuInSe_2$ film in contact with KCl solution (pH ~2). The CISe film was prepared by pulsed electrodeposition, using $E_1 = -0.9\,V_{SCE}$, then annealed in argon and etched 5 min in KCN solution. The frequency was 1 kHz and the sweep rate 10 mV s^{-1}.

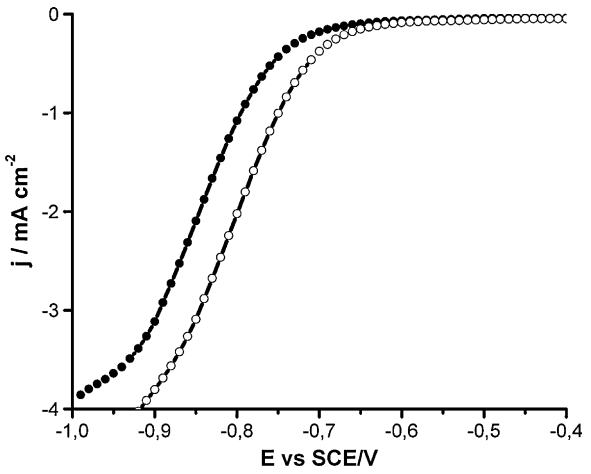

Fig. 10. Polarization curve of $CuInSe_2$ film in contact with KCl solution (pH ~2) in dark (black circles) and under illumination (white circles). The CISe film was prepared by pulsed electrodeposition, using $E_1 = -0.9\,V_{SCE}$. It was then annealed in argon and etched in KCN solution.

for a p-type semiconductor, A the surface area of the sample, V the electrode potential, and V_{FB} the flatband potential. The dielectric constant ε is taken as 8.1 [26]. Fig. 9 shows a MS plot of an annealed sample prepared by pulsed ED, where the negative slope confirms p-type conductivity. The intercept on the applied potential axis yields −0.6 V for the flat band potential. The acceptor density (N), calculated from the slope, resulted in $4 \times 10^{19}\,cm^{-3}$. Even if this value is higher than expected, it has to be taken into account that most of the data in the literature apply to ingots [28] or monocrystalline CISe [29]. Instead, these samples are polycrystalline, where due to the presence of grain borders and surface states, the number of defects can increase noticeably. Also, roughness might increase the active area. Other authors have found similarly high values of carrier density in electrodeposited CISe films. This fact has been related to a high density of defects present in the film [26] or to remnant secondary phases of Cu_xSe that are located deeper in the material and are not effectively removed by KCN etching [30]. Other studies [18,31] report carrier density values obtained using solid-state devices, in contrast with our measurements, which are performed in solution, using a conventional three-electrode cell. Lower donor densities calculated in air when compared to those measured in electrolyte-filled TiO_2 electrodes have been reported before by other authors and attributed to increased oxygen vacancy passivation in air [32]. The potentiodynamic polarization curves, recorded in the dark and under illumination after the annealing treatment, are shown in Fig. 10. The dark current density (J_d) is relatively small (of about 0.1 μA) indicating that CISe forms a blocking contact with the electrolyte. Upon irradiation, the curve exhibits a cathodic photocurrent J_{ph} supporting the p-type character as expected for the Cu-rich side in the ternary Cu–In–Se phase diagram [25,28]. As anticipated, the onset of the photocurrent is in good agreement with the flat band potential that can be derived from the Mott-Schottky plot ($E_{FV} = -0.58\,V_{SCE}$) according to the relation that $J_{ph} \propto (V_{FB} - V)$ [27]. Other authors have found similar results in electrodeposited p-type CISe films [28].

4. Conclusions

$CuInSe_2$ films were electrodeposited onto FTO glass from a single bath, comparing two-step potential pulses with potentiostatic electrodeposition. Two different potential values were investigated.

There are slight differences in film morphology and coverage when depositing at −0.7 or $-0.9\,V_{SCE}$, although the reasons that

explain this effect are still unclear. However, they both improve distinctly by pulsing the potential and even more by annealing.

EDS and micro-Raman maps demonstrate that the composition is spatially homogeneous when the potential is pulsed. Also, the presence of secondary phases is much lower than that on films prepared at fixed potentials. The amount of residual elemental Se is greatly decreased during the thermal treatment while Cu_xSe can only be efficiently removed by etching in KCN solution. Only after annealing the samples are crystalline enough so as to show distinctive peaks in the X-ray diffractograms. Overall, there seems to be no noticeable quality differences between the films prepared by pulsing the potential at −0.7 or 0.9 V. Instead the global composition seems to be better adjusted when pulsing the potential, in contrast with fixing the potential.

Photoelectrochemical tests, polarization curves and Mott-Schottky plots confirm p-type conduction. These, together with absorption spectra enable the calculation of relevant semiconductor parameters such as band gap energy, flat band potential and carrier's density. The properties obtained suggest that electrodeposition is suitable to prepare photovoltaic devices, but the photocurrent is higher when the potential is pulsed.

The diffusion regime imposed by the potential pulses could be responsible for the differences in morphology and composition. Further research will focus on using pulsed electrodeposition to infiltrate nanoporous oxides and to prepare 3D-solar cells.

Acknowledgments

The authors acknowledge the financial support received from Consejo Nacional de Investigaciones Científicas y Técnicas (CONICET), Agencia Nacional de Promoción Científica y Tecnológica (AGENCIA) and Universidad Nacional de Mar del Plata (UNMdP) from Argentina.

References

[1] M. Kemell, M. Ritala, M. Leskelá, Crit. Rev. Solid State 30 (2005) 1.
[2] Q. Wang, K. Zhu, N.R. Neale, A.J. Frank, Nano Lett. 9 (2009) 806.
[3] S. Phok, S. Rajaputra, V.P. Singh, Nanotechnology 18 (2007).
[4] M. Nanu, J. Schoonman, A. Goossens, Adv. Mater. 16 (2004) 453.
[5] M. Nanu, J. Schoonman, A. Goossens, Adv. Funct. Mater. 15 (2005) 95.
[6] F. Kang, J.P. Ao, G.Z. Sun, Q. He, Y. Sun, Mater. Chem. Phys. 115 (2009) 516.
[7] M.A. Frontini, M. Vázquez, J. Mater. Sci. 45 (2010) 2995.
[8] C.J. Hibberd, E. Chassaing, W. Liu, D.B. Mitzi, D. Lincot, A.N. Tiwari, Prog. Photovoltaics 18 (2010) 434.
[9] J.F. Guillemoles, P. Cowache, A. Lusson, K. Fezzaa, F. Boisivon, J. Vedel, D. Lincot, J. Appl. Phys. 79 (1996) 7293.
[10] D. Lincot, J.F. Guillemoles, S. Taunier, D. Guimard, J. Sicx-Kurdi, A. Chaumont, O. Roussel, O. Ramdani, C. Hubert, J.P. Fauvarque, N. Bodereau, L. Parissi, P. Panheleux, P. Fanouillere, N. Naghavi, P.P. Grand, M. Benfarah, P. Mogensen, O. Kerrec, Sol. Energy 77 (2004) 725.
[11] F. Kang, J. Ao, G. Sun, Q. He, Y. Sun, J. Alloys Compd. 478 (2009) L25.
[12] Y.P. Fu, R.W. You, K.K. Lew, J. Electrochem. Soc. 156 (2009) D553.
[13] A. Palacios-Padrós, F. Caballero-Briones, F. Sanz, Electrochem. Commun. 12 (2010) 1025.
[14] M. Valdés, M.A. Frontini, M. Vázquez, A. Goossens, Appl. Surf. Sci. 254 (2007) 303.
[15] International Centre for Diffraction Data (ICCD): Powder Diffraction File Database, in, Newtown Square, EEUU, 1998.
[16] M.E. Calixto, K.D. Dobson, B.E. McCandless, R.W. Birkmire, J. Electrochem. Soc. 153 (2006) G521.
[17] S.H. Kang, Y.-K. Kim, D.-S. Choi, Y.-E. Sung, Electrochim. Acta 51 (2006) 4433.
[18] P.J. Dale, A.P. Samantilleke, G. Zoppi, I. Forbes, L.M. Peter, J. Phys. D Appl. Phys. 41 (2008).
[19] V. Izquierdo-Roca, A. Pérez-Rodríguez, A. Romano-Rodríguez, J.R. Morante, J. Alvarez-García, L. Calvo-Barrio, V. Bermudez, P.P. Grand, O. Ramdani, L. Parissi, O. Kerrec, J. Appl. Phys. 101 (2007).
[20] C. Rincón, F.J. Ramírez, J. Appl. Phys. 72 (1992) 4321.
[21] O. Ramdani, J.F. Guillemoles, D. Lincot, P.P. Grand, E. Chassaing, O. Kerrec, E. Rzepka, Thin Solid Films 515 (2007) 5909.
[22] R. Noufi, R. Axton, C. Herrington, S.K. Deb, Appl. Phys. Lett. 45 (1984) 668.
[23] S.B. Zhang, S.H. Wei, A. Zunger, Phys. Rev. Lett. 78 (1997) 4059.
[24] Y. Ueno, H. Kawai, T. Sugiura, H. Minoura, Thin Solid Films 157 (1988) 159.
[25] T. Edamura, J. Muto, J. Mater. Sci. Mater. 5 (1994) 275.
[26] R.P. Raffaelle, H. Forsell, T. Potdevin, R. Friedfeld, J.G. Mantovani, S.G. Bailey, S.M. Hubbard, E.M. Gordon, A.F. Hepp, Sol. Energy Mater. Sol. C 57 (1999) 167.
[27] N. Sato, Electrochemistry at Metal and Semiconductor Electrodes, Amsterdam, 1998.
[28] L. Djellal, A. Bouguelia, M. Trari, Mater. Chem. Phys. 109 (2008) 99.
[29] H.C. Du, C. Shih, Thin Solid Films 480–481 (2005) 37.
[30] M. Kemell, Electrodeposition of $CuInSe_2$ and doped ZnO thin films for solar cells, in: Laboratory of Inorganic Chemistry, Department of Chemistry, Faculty of Science, PhD thesis, University of Helsinki, Helsinki, 2003.
[31] S.N. Qiu, L. Li, C.X. Qiu, I. Shih, C.H. Champness, Sol. Energy Mater. Sol. C 37 (1995) 389.
[32] R. O'Hayre, M. Nanu, J. Schoonman, A. Goossens, J. Phys. Chem. C 111 (2007) 4809.